THE AMERICAN SOCIETY OF MECHANICAL ENGINEERS
345 E. 47 St., New York, N.Y. 10017

87-GT-7

Failure Prediction of Hot-Pressed Si_3N_4 Ceramics by NDE

J. P. SINGH, R. A. ROBERTS, J. J. VAITEKUNAS, and W. A. ELLINGSON
Materials and Components Technology Division
Argonne National Laboratory
Argonne, Illinois 60439

ABSTRACT

Results are presented on the detection of critical flaws in hot-pressed Si_3N_4 with Fe inclusions by nondestructive evaluation (NDE) and fractographic observation. The NDE methods employed included (1) low-energy contact radiography with digital image enhancement and (2) through-transmission and backscatter ultrasonic imaging. A comparison of NDE and fractography results indicates that the backscatter ultrasonic method may be more suitable than low-kV contact radiography for the detection of near-surface flaws.

INTRODUCTION

Ceramic materials such as Si_3N_4, SiC, and ZrO_2 are playing an ever-increasing role in structural applications because of their potentially excellent high-temperature mechanical properties as well as good corrosion and thermal-shock resistance. However, a primary factor influencing their use in structural applications is mechanical reliability.[1,2] It has been observed that the mechanical properties of these ceramics are generally controlled by surface and internal flaws[3,4] such as machining flaws, pores, inclusions, density gradients, and other microstructural irregularities. These flaws are introduced during fabrication and machining.[4-6] Successful application of NDE to detect these flaws in ceramic parts during both fabrication and final inspection will be very cost effective and will serve as a key tool in achieving increased reliability. A number of NDE techniques are being developed to detect such flaws.[7-10] These include x-ray computed tomography, x-ray microradiography, through-transmission ultrasound, backscatter ultrasound, spin-echo nuclear magnetic resonance imaging, and dye penetrant methods.

The selection of a particular NDE technique for flaw detection or characterization depends upon the state of the ceramic (green or dense) and the nature of the flaws or characteristic to be studied, i.e., surface flaws such as cracks and inclusions or internal flaws such as inclusions, pores, agglomerates, and density gradients. For improved quality assurance, the relative sensitivity of each of the NDE techniques for flaw detection needs to be evaluated at critical steps in the ceramic processing. Furthermore, it has been observed that use of NDE methods optimized for metals is not acceptable for some ceramic materials. Extensive development of the NDE methods is needed in order to optimize the ceramic process steps as well as to detect failure-initiating flaws in ceramic components.

This paper gives the results of a limited flaw detection study involving two different NDE techniques, low-energy contact x-radiography and focused ultrasonic imaging. Because inclusions rich in Fe and Si have been observed[11-14] to cause substantial strength degradation of Si_3N_4 material, this initial study was conducted on a Si_3N_4-Fe system. Internal inclusions (flaws) were introduced by adding controlled amounts of Fe particles to the Si_3N_4 before hot pressing. Results of experiments to detect strength-limiting flaws by NDE inspection were subsequently compared with fractographic observations to evaluate the relative effectiveness of the NDE techniques.

EXPERIMENTAL DETAILS

Specimen Preparation

The specimens used in this study were hot-pressed Si_3N_4 disks (~3.8 cm in diam x 0.4 cm thick) made from GTE SN-502 Si_3N_4 powder with 6 wt % Y_2O_3 as a densification aid. To simulate flaws, 5 wt % Fe (88-125 μm particles) was added to the powder mixture. The disks were pressed in a boron-coated graphite die at 1725°C and 22 MPa for 2 h in a high-purity N_2 atmosphere. The density of the hot-pressed disks was ~3.25 g/cm (~98.5% theoretical). Following removal from the die, the disks were surface ground with a 32-μm diamond grit wheel. Modulus of rupture (MOR) bars (~3.8 x 0.4 x 0.4 cm) were subsequently machined from these disks for fracture and fractographic studies.

Presented at the Gas Turbine Conference and Exhibition, Anaheim, California — May 31-June 4, 1987

NDE Approach

Nondestructive evaluation was performed on the hot-pressed Si_3N_4 specimens before and after machining of the MOR bars from the hot-pressed disks. The techniques used were low-energy contact x-radiography and focused through-transmission ultrasonic imaging. NDE data collected on the hot-pressed disks were used to determine the orientation of the cutting lines for the MOR bars. The objective was to place detected major silicon, iron and/or iron-rich inclusions (critical flaws) in the constant-moment cross section, as loading was to be done using four-point-bend tests.

Discussion of Ultrasonic Methods

Ultrasonic through-transmission images of both the Si_3N_4 disks and MOR bars were obtained with a pair of focused 25-MHz broadband transducers in an immersion configuration. The ~200-μm-diam focal zone of the focused ultrasonic field was scanned throughout the specimen in a rectangular grid covering the specimen surface. The amplitudes of through-transmitted broadband ultrasonic pulses were digitally recorded at each discrete scan position (pixel), and the pulse amplitude was displayed (as a gray scale) on a video monitor as an ultrasonic image. For the complete disk specimens, through-transmission data were recorded at 448 x 448 discrete points separated by a 100-μm step size. Images therefore cover a 44.8 x 44.8 mm area. Images of the MOR bars were obtained with the same ultrasonic system, but they comprised 384 x 96 pixels covering a 38.4 x 9.6 mm area. The through-transmission ultrasonic images display inclusions, voids, cracks, etc., throughout the thickness of the specimen. However, it is noted in fracture studies with four-point bend loading that failure generally originates at defects near the tensile surface of the MOR bar. Therefore, in addition to through-transmission imaging, ultrasonic backscatter images of the tensile surface* of the MOR bars were obtained with a single focused 25-MHz transducer in a pulse-echo mode. The transducer was focused just below the surface of the specimen at a nonperpendicular angle of incidence. The angle of incidence was chosen so as to optimize surface wave generation. In the presence of near-surface defects, the generated surface waves are reflected back to the ultrasonic transducer where they are detected. The technique is primarily sensitive to defects within a depth of one surface wavelength (approximately 200 μm at 25 MHz). Backscatter images of the MOR bars are obtained on a 384 x 96 grid covering the specimen surface.

Discussion of X-Radiographic Methods

Contact x-radiographic images were obtained on both the complete Si_3N_4 disks and the individual MOR bars. We chose to use as low an x-ray head accelerating voltage as possible in order to increase the low-energy photon contribution to the x-ray image, as this improves the contrast resolution. Our x-ray imaging protocol was based on earlier work by Smith,[15] who suggested that for specimens of sizes relevant to the present study, projection radiography provides very little increase in contrast over contact radiography for the case of Fe inclusions in a Si_3N_4 matrix. This is also in agreement with recent work by Baaklini,[16] who has suggested that microfocus radiography (~20-μm focal spot size) provides excellent detection of flaws with high differential contrast (e.g., voids or Fe inclusions in a Si_3N_4 matrix). Baaklini reported a 95% probability of detection of voids in Si_3N_4 specimens up to 10 mm thick.

We implemented the contact radiographic method using an ordinary Picker-110 "hot shot" which has a fixed tungsten anode and a 250 μm beryllium window. The focal spot size of the x-ray head is stated by the manufacturer to be ~500 μm, but we had no way to verify this. The filament current was kept to nominally 5 mA in all cases. The film used was Kodak Type M Redi-Pak which incorporates a 0.005 in. Pb screen to reduce scattered radiation. Optical film densities were kept to nominally three in order to increase contrast sensitivity. The source-to-film distance was kept at 14 in. and the imaging times were 5-6 min.

Fracture and Fractography

The MOR bars were fractured in a four-point bending mode in an Instron machine with a crosshead speed of 0.127 cm/min. The bars were positioned in such a way that the apparent critical flaws (inclusions) detected by NDE were located in a tensile region. The fracture surfaces of the broken bars were examined by optical and scanning electron microscopy to locate critical flaws. An optical microscope at low magnification was used to find the general locations of critical flaws by identifying fracture markings[17,18] such as fracture mirror and river patterns. Subsequently, a scanning electron microscope was used to find the exact location and examine the details of critical flaws.

RESULTS AND DISCUSSION

Comparison of X-Ray and Ultrasound Images

In order to compare the data from the two NDE imaging modalities, the x-ray images were digitized using a 512 x 512 matrix, with a Sony charge-coupled device (CCD) camera. The ultrasonic images were already in digital format. These two image modalities were then compared by simultaneously displaying these images using an IBM PC coupled to a split screen with a 512 x 512 display capability. When the user moves a mouse-activated cursor over one of the two images, the computer automatically displays a second cursor at the corresponding point on the other image. A comparison of typical x-ray and ultrasonic images of a Si_3N_4 disk containing 5 wt % Fe inclusions is presented in Fig. 1. Several corresponding image features are noted. Agreement between the imaging modalities is quite good. The x-ray image has a high contrast and thus sharp detail is apparent. The apparent blurring of the ultrasonic image is caused largely by the high concentration of iron inclusions.

A comparison of x-ray and ultrasound images of a MOR bar is presented in Fig. 2. Corresponding image features are marked in the x-ray and through-transmission ultrasound images. Again, a sharper contrast is seen in the x-ray image than in the through-transmission ultrasound image. The effectiveness of ultrasonic backscatter in detecting near-surface flaws, as opposed to internal flaws, is demonstrated in the backscatter image of Fig. 2. In this image, the features representing the inclusions have

*Note: The surface to be placed in tension during the four-point load was determined a priori by using the NDE data from the individual MOR bars.

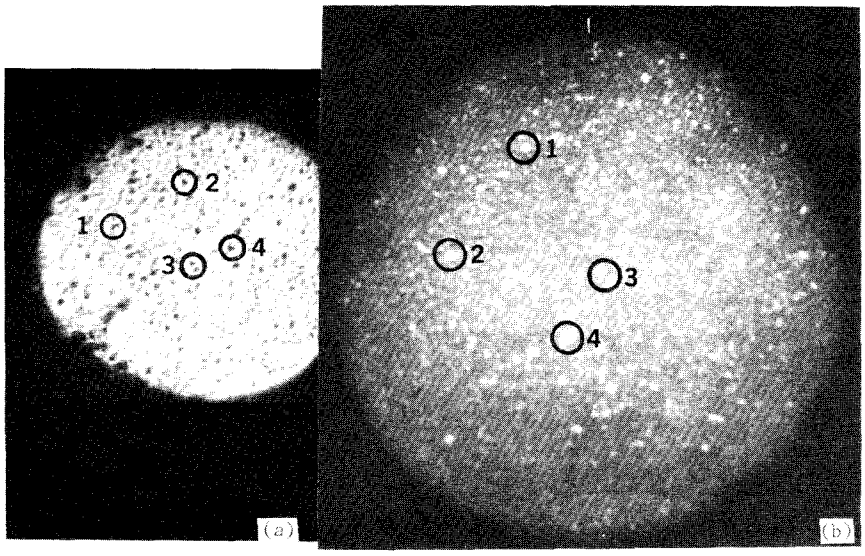

Fig. 1. Comparison of (a) Through-Transmission Ultrasound and (b) Low-kV X-Ray Images of a Si_3N_4 Disk Containing 5% Fe Inclusions. Some of the flaws (inclusions) found in both images are indicated by markers.

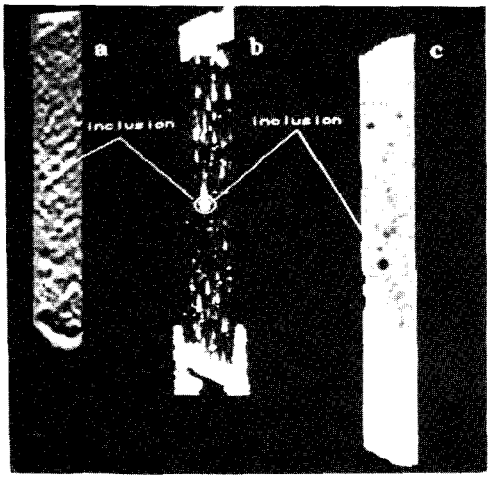

Fig. 2. Comparison of (a) Through-Transmission Ultrasound, (b) Backscatter Ultrasound, and (c) Low-kV X-Ray Images of a Modulus of Rupture Bar. Common image features are indicated.

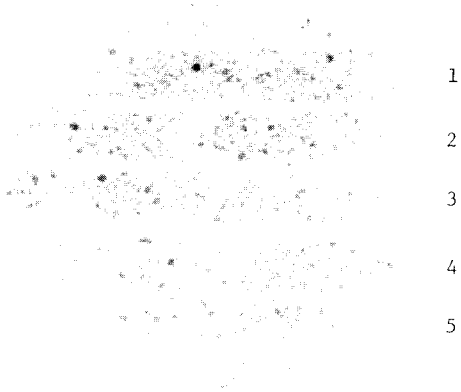

Fig. 3. An X-Ray Image of One of the Si_3N_4 Disks with 5% Fe Inclusions, Showing the Relative Orientation of Modulus of Rupture Bars.

elongated "tails" which arise from the strong reflection of surface waves as the focused beam approaches the inclusion. Other image features, which lack these tails, likely indicate less critical topographical features.

Correlation of NDE and Fractographic Observations

Initial effort concentrated on correlating fractographic observations with NDE data for the detection of critical flaws. The indicated features in Fig. 1 (presumed to be Si, Fe, and/or Fe-rich inclusions) were selected to be critical flaws, and MOR bars (Fig. 3) were machined accordingly from the disks. The MOR bars were loaded to fracture in flexural mode (four-point bending), with the critical (largest) flaws positioned in the tensile region. The fracture surfaces of the broken MOR bars were then examined by fractography to locate critical flaws. In each case, the fracture initiated from an internal flaw located within ~150 μm of the tensile surface. As indicated by energy-dispersive x-ray analysis (EDAX), these flaws were primarily Si- and Fe-rich inclusions and regions of Si_3N_4 matrix, that showed evidence of degradation, probably as a result of the reaction between Si_3N_4 and molten Fe. Figure 4 shows an example of such a flaw, which caused failure in MOR bar #1 of Fig. 3. The critical-flaw locations predicted by NDE agreed with fractographic observations for 5 out of 14 MOR bars. For these five bars, the critical flaws predicted by low-kV radiography and through-transmission ultrasound were at or near the

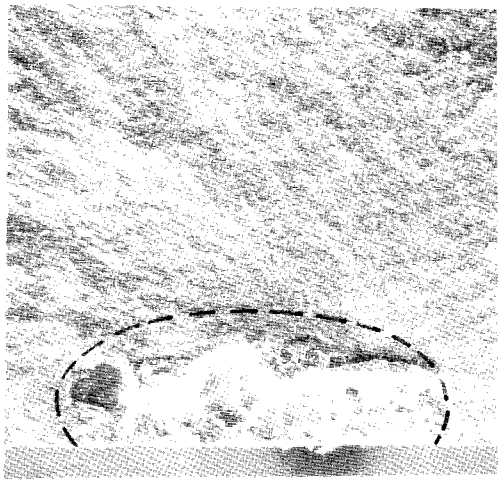

Fig. 4. Scanning Electron Micrograph of Fracture Surface of Modulus of Rupture Bar #1 in Fig. 3. The micrograph shows a critical flaw (Si-rich inclusion) within the dashed line. Magnification, 110X.

tensile surface. For the other bars, the large flaws that were predicted to be critical were farther from the tensile surface than the actual failure-initiating flaws. Therefore, although the largest inclusions were detected in these specimens, the tensile stress and hence the stress intensity factor at those inclusions were not sufficient to cause failure.

In view of the above discussion, for ceramic components subject to large tensile stresses near the surface, failure can be expected to initiate from near-surface flaws. In this case, backscatter ultrasound may be the desired NDE method because this technique is only sensitive to near-surface flaws. In contrast, low-kV contact radiography and through-transmission ultrasound do not discriminate between near-surface and internal flaws, as seen in Fig. 2. Also, as expected, for reliable NDE prediction of a "critical" flaw (inclusion, void, crack, etc.), the state of stress at flaw locations must be taken into account.

ACKNOWLEDGMENTS

The research was supported by the U. S. Department of Energy, Advanced Research and Technology Development Fossil Energy Materials Program, under contract W-31-109-Eng-38. Thanks are extended to J. Lucas of the Quality Assurance Division for helping with the radiographic imaging, and to R. B. Poeppel, Manager of the Ceramics Section, for frequent discussions and helpful comments.

REFERENCES

1. Ceramic Technology Program for Advanced Heat Engines Program Plan, Oak Ridge National Laboratory Report ORNL/TM-8896 (June 1984).
2. Rice, R. W., An Assessment of the Use of Ceramics in Heat Engines, U. S. Naval Research Laboratory NRL Memorandum Report 4499 (March 1981).
3. Reliability of Ceramics for Heat Engine Applications, National Materials Advisory Board Report NMAB-357 (1980).
4. Lange, F. F., "Processing-Related Fracture Origins: 1. Observations in Sintered and Isostatically Hot-Pressed Al_2O_3/ZrO_2 Composites," J. Am. Ceram. Soc. 66(6), 396-398 (1983).
5. Singh, J. P., Argonne National Laboratory, unpublished work.
6. Rice, R. W., Mecholsky, J. J., Freiman, S. W., and Morey, S., "Failure Causing Defects in Ceramics: What NDE Should Find," U. S. Naval Research Laboratory NRL Memorandum Report 4075 (1979).
7. Ellingson, W. A., Roberts, R. A., and Vannier, M. W., "Recent Results Comparing Low-kV Radiography, Ultrasound, and Computed Tomography for Flaw Detection in Dense Ceramics," Mater. Eval. 44(9), 35P (1986).
8. Roberts, R. A., Ellingson, W. A., and Vannier, M. W., "Recent Results Comparing Low-kV Radiography, Ultrasound, and Computed Tomography for Flaw Detection in Green-State Ceramics," to be published in Proc. 15th Symp. on Nondestructive Evaluation, Southwest Research Institute, San Antonio, TX, 1985.
9. Ackerman, J. L., Ellingson, W. A., Kontcher, J. A., and Rosen, B. R., "Development of Nuclear Magnetic Resonance Imaging Techniques for Characterizing Green-State Ceramic Materials," to be published in Proc. 2nd Intl. Symp. on Nondestructive Characterization of Materials, Montreal, Canada, July 21-23, 1986.
10. Taylor, T., Ellingson, W. A., and Koenigsberg, W. P., "Evaluation of Engineering Ceramics by Gamma-Ray Computed Tomography," Atomic Energy of Canada Limited, Report AECL-9005 (January 1986).
11. Pasto, A. E., Neil, J. T., and Quackenbush, C. L., "Microstructural Effects Influencing Strength of Sintered Silicon Nitride," pp. 476-489 in Ultrastructure Processing of Ceramics, Glasses, and Composites, edited by L. L. Hench and D. R. Ulrich, John Wiley, New York (1984).
12. Pasto, A. E., "Causes and Effects of Fe-bearing Inclusions in Sintered Si_3N_4," Comm. Am. Ceram. Soc. 67(8), C178-C180 (1984).
13. Singh, J. P., "Effect of Flaws on Fracture Toughness of Structural Ceramics," pp. 299-305 in AR&TD Fossil Energy Materials Program Quarterly Progress Report for the Period Ending September 30, 1985, ORNL/FMP-85/4 (1985).
14. Baumgartner, H. R., and Richerson, D. W., "Inclusion Effects on the Strength of Hot-Pressed Si_3N_4," pp. 367-386 in Fracture Mechanics of Ceramics, Vol. 1, edited by R. C. Bradt, D. P. H. Hasselman, and F. F. Lange, Plenum Press, New York (1973).
15. Smith, R. L., "The Effect of Scattering on Contrast in Microfocus Projection X-radiography," Bri. J. Non-Destr. Test. 22(1), 236-239 (1980).
16. Baaklini, G. Y., Kiser, J. D., and Roth, D. J., "Radiographic Detectability Limits for Seeded Voids in Sintered Silicon Carbide and Silicon Nitride," Adv. Ceram. Mater. 1(1), 43-49 (1986).
17. Johnson, J. W., and Holloway, D. G., "On the Shape and Size of the Fracture Zones on Glass Fracture Surfaces," Phil. Mag. 14, 731-743 (1966).
18. Mecholsky, J. J., Freiman, S. W., and Rice, R. W., "Fracture Surface Analysis of Ceramics," J. Mater. Sci. 11, 1310-1319 (1976).